09.4

Optical studies of InP/InAsP/InP nanoinclusions integrated into silicon

© I.A. Melnichenko [1,2], S.D. Komarov [1], A.S. Dragunova [1], A.A. Karaborchev [1], E.I. Moiseev [1], N.V. Kryzhanovskaya [1], I.S. Makhov [1], A.E. Zhukov [1]

[1] National Research University Higher School of Economics, St. Petersburg, Russia
[2] Alferov Federal State Budgetary Institution of Higher Education and Science Saint Petersburg National Research Academic University of the Russian Academy of Sciences, St. Petersburg, Russia
E-mail: imelnichenko@hse.ru

Received November 13, 2023
Revised November 15, 2023
Accepted November 15, 2023

Submicron $InAs_xP_{1-x}$/InP nanoinclusions formed by selective epitaxial growth in silicon using metal & — organic vapor epitaxy and a molten drop of a group III element have been studied using confocal optical microscopy and microphotoluminescence spectroscopy. The influence of the distance between nanoinclusions on the photoluminescence intensity was investigated, and the temperature dependences of photoluminescence in the range of 77−290 K were obtained. Emission in the spectral range of 1.2 μm was obtained at room temperature.

Keywords: A3B5 nanoinclusions, InAsP integration on silicon, InAsP/InP.

DOI: 10.61011/PJTF.2024.05.57175.19801

The development of techniques for integration of emitting A3B5 nanoinclusions with silicon is of paramount importance in photonics. Having solved this problem, one may proceed to integrating the technology of high-speed protected optical data transmission with the well-developed silicon integrated circuit technology for subsequent application in high-throughput big data processing systems, quantum computation, and cryptography. The difficulty of monolithic epitaxial synthesis of A3B5 nanoinclusions with high radiative recombination efficiency on silicon platform primarily from the mismatch between lattice parameters that leads to fabrication of structures with defect (threading dislocations, microcracks, antiphase boundaries) densities exceeding the levels acceptable for device engineering. Methods proposed for overcoming these difficulties involve the application of special buffer layers (dislocation filters) [1], misoriented [2] or structured [3] substrates, and heterogeneous (hybrid) integration based on bonding [4] and transfer printing [5]. Selective growth [6] techniques and methods for nanostructure growth with the use of catalyst droplets [7] are advancing rapidly.

A novel method for selective epitaxial growth of A3B5 on silicon with the use of metalorganic vapor-phase epitaxy (MOVPE) and a molten droplet of a group III element (molten alloy driven selective-area growth, MADSAG) [8] has been proposed recently. Sidestepping the application of complex bonding techniques, it provides an opportunity to implement accurate matching of A3B5 components and silicon at the microlevel. Group III element droplets are deposited first into pits etched on the silicon surface, and subsequent MOVPE annealing in group V precursor vapor ensures crystallization of each droplet. This method combines the advantages of selective and droplet growth: exact positioning of nanoinclusions and growth selectivity are matched with a fine degree of control over nucleation in the liquid phase. In the present study, the influence of distance between pits etched on the silicon surface on the optical characteristics of $InAs_xP_{1-x}$/InP nanoinclusions synthesized by MADSAG is examined by mapping the surface via confocal optical microscopy at room temperature and microphotoluminescence (micro-PL) spectroscopy within the 77−290 K temperature range.

The studied heterostructures were synthesized by MOVPE on a Si substrate with crystallographic orientation (001). Prior to epitaxial growth, a SiN_x mask 50 nm in thickness was formed on the silicon surface by plasma-chemical deposition. A mask pattern of round pits was formed by deep ultraviolet lithography. The distance between centers of pits (pitch) etched in different samples was 400, 600, or 800 nm. The diameter of each pits at its top was 200 nm. Deep reactive ion etching in sulfur hexafluoride (SF_6) was used to form pits with a depth of 200 nm in silicon. Additional liquid anisotropic etching in KOH resulted in the formation of another pyramidal pits edged by the {111} planes of silicon. Epitaxial growth began with the formation of an InP layer inside pits, which was then covered with $InAs_xP_{1-x}$. The $InAs_xP_{1-x}$ layer growth procedure was repeated five times in order to enhance the uniformity of pits filling and increase the amount of emitting material. A top InP layer covering the structure was formed at the final stage. The technological aspects of growth of nanoinclusions were discussed in more detail in [8,9].

Micro-PL maps of nanoinclusions were compiled using an NTEGRA Spectra optical confocal microscope. An Nd:YLF continuous-wave pump laser operating at a wavelength of 527 nm was used for excitation. Its emission was focused by a microobjective (100×, Mitutoyo, M Plan APO NIR, NA=0.5). A measurement system including cooled Si and InGaAs CCD detectors (Andor) and a MS5204i (Sol

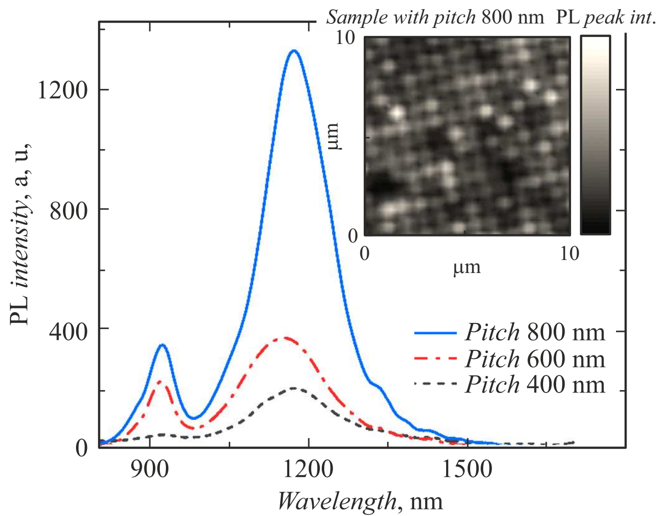

Figure 1. Room-temperature micro-PL spectra for structures with $InAs_xP_{1-x}$ nanoinclusions with a pitch of 800, 600, and 400 nm. A map of the integral micro-PL intensity distribution within the 1100–1260 nm wavelength range for an array of $InAs_xP_{1-x}$/InP nanoinclusions with a pitch of 800 nm is shown in the inset.

Instruments) monochromator was used for signal detection. The optical pump power was ~ 1.7 mW, and the pump spot diameter was $0.7\,\mu$m. In order to examine their optical properties within the 77–290 K temperature range, the studied structures were introduced into a Janis ST-500 cryostat.

The room-temperature micro-PL spectra (Fig. 1) recorded at the sites with $InAs_xP_{1-x}$ nanoinclusions in ordered pits contain a line with its maximum positioned at a wavelength of approximately 915 nm and a broader line with a maximum around 1200 nm. These lines correspond to carrier recombination in InP and $InAs_xP_{1-x}$ emission, respectively. In our view, the large spectral width of the second line is indicative of inhomogeneity of composition of the $InAs_xP_{1-x}$ solid solution in a nanoinclusion. The positions of micro-PL maxima of individual nanoincluisions fall within the 1180–1220 nm (1.051–1.016 eV) spectral range, which corresponds to a mean arsenic concentration of 28–31%.

A map of the integral micro-PL intensity distribution (1100–1260 nm) at room temperature for an array of nanoinclusions with a pitch of 800 nm is shown in the inset of Fig. 1. Ordered bright dots represent the emission of individual nanoinclusions. It follows from the intensity distribution that emission is observed from the majority of $InAs_xP_{1-x}$ nanoinclusions: in average, only 12–15 out of 100 nanoinclusions produce a weak luminescence signal. Virtually no emission is detected within the entire wavelength range between the bright dots. This indicates that InAsP does not get deposited onto the SiN_x surface between pits due to diffusion of the deposited material from this region into ordered pits. Scanning electron microscope (SEM) images of the sample with a pitch of 800 nm (Fig. 2, *a*) also reveal an ordered array of nanoinclusions with their top layer protruding above the silicon surface.

The intensity of the micro-PL signal from nanoinclusions drops when the distance between pits centers decreases from 800 to 400 nm (Fig. 1). It is our belief that this is caused by a reduction in the amount of material per a pits and the corresponding reduction in the pits fill factor. This hypothesis is verified by SEM images (Fig. 2, *b*). Thus, further optimization of the amount of deposited material coupled with monitoring of pits filling are needed to form a denser array of nanoinclusions.

The temperature dependence of photoluminescence (Fig. 3, *a*) was examined in order to characterize the optical quality of the material of $InAs_xP_{1-x}$/InP nanoinclusions formed with the optimum period of 800 nm. The integral intensity dropped by a factor of 23 as the temperature grew from 77 to 290 K. This is indicative of a moderate level of non-radiative recombination in the epitaxial structure, since the obtained result is comparable to the data for structures synthesized on native (InP) substrates [10]. The spectral shift of wavelength of the photoluminescence maximum with an increase in temperature is presented in Fig. 3, *b*. The theoretical curve characterizing the band gap variation of solid solution $InAs_xP_{1-x}$ with temperature was plotted in accordance with Varshni formula

$$Eg^{InAs_xP_{1-x}}(T,x) = \left(Eg_0^{InAs} - \frac{\alpha_{InAs}T^2}{\beta_{InAs}+T}\right)x + \left(Eg_0^{InP} - \frac{\alpha_{InP}T^2}{\beta_{InP}+T}\right)(1-x) + Cgx(1-x),$$

where parameters α_{InAs}, β_{InAs} and α_{InP}, β_{InP} were set to $2.5\cdot10^{-4}$ eV/K [10], 162 K and $3.63\cdot10^{-4}$ eV/K, 75 K [11], respectively, bowing parameter $C = 0.1$ eV [12], and $x = 0.3$. It is evident that the theoretical curve provides a close fit to experimental data, indicating a lack of clusters differing strongly in their chemical composition in the $InAs_xP_{1-x}$ solid solution.

We note in conclusion that, for practical purposes, the discussed selective growth of A3B5 emitters may also be performed on a silicon-on-insulator wafer. The Si/SiO_2 optical contrast should provide an opportunity to form three-dimensional microcavities with A3B5 nanoinsertions positioned in a controlled manner in them. This control over the positioning of nanoinsertions in a cavity may be used to adjust the direction pattern of a microlaser, modulate losses, and alter the factor of overlapping of the optical mode with the active region; in addition, quantum-dimensional insertions may potentially enable the production of single-photon sources.

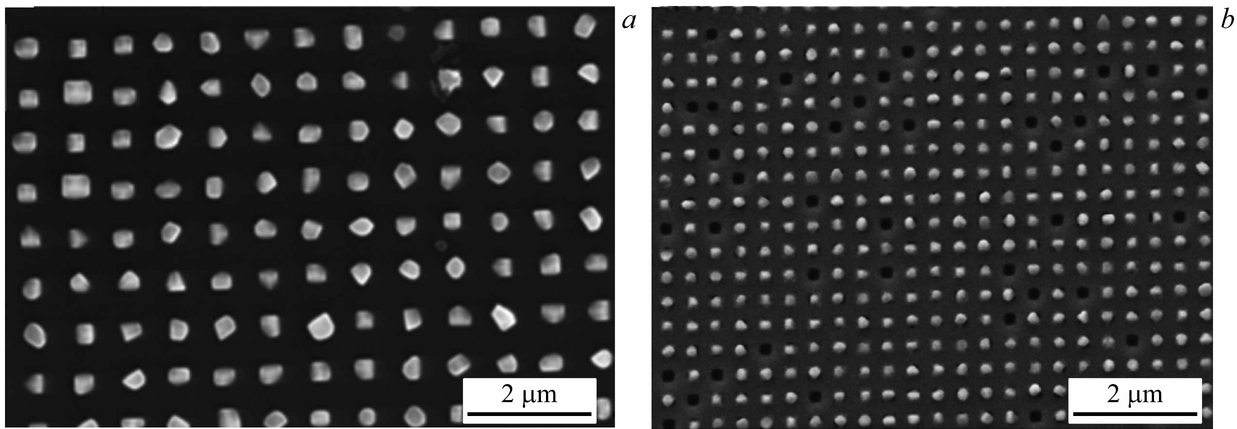

Figure 2. SEM images of the surface of silicon with $InAs_xP_{1-x}$/InP nanoinclusions with a pitch of 800 (*a*) and 400 nm (*b*).

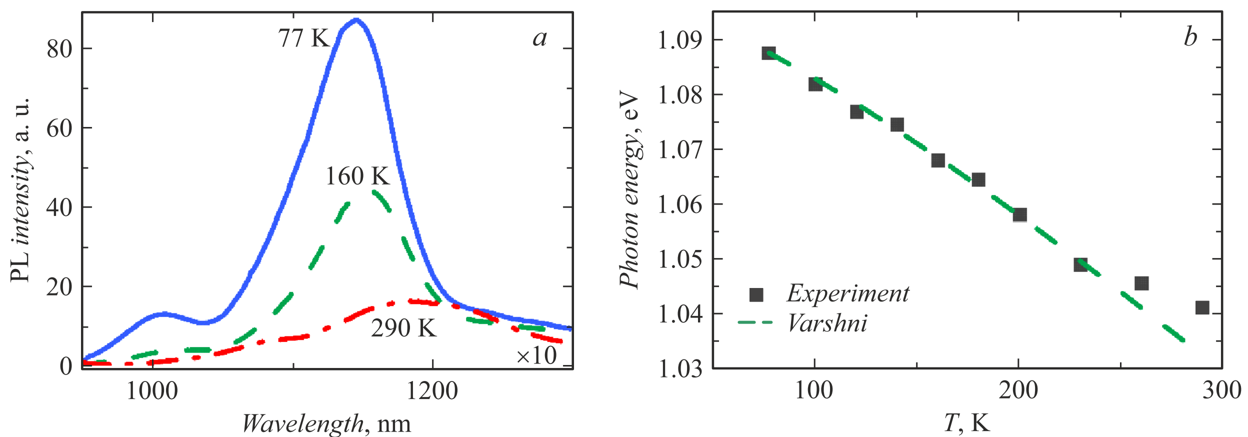

Figure 3. *a* — micro-PL spectra for a structure with a nanoinclusion pitch of 800 nm at temperatures of 77–290 K; *b* — temperature dependence of the micro-PL intensity maximum and theoretical Varshni curve for $InAs_xP_{1-x}$.

Acknowledgments

The authors wish to thank E. Semenova and D. Vyazmitinov for providing the studied structures.

Funding

This study was supported by grant No. 22-22-20057 from the Russian Science Foundation (https://rscf.ru/project/22-22-20057) and a grant from the St. Petersburg Science Foundation under agreement No. 66/2022 dated April 15, 2022.

Conflict of interest

The authors declare that they have no conflict of interest.

References

[1] M. Tang, J.-S. Park, Z. Wang, S. Chen, P. Jurczak, A. Seeds, H. Liu, Prog. Quantum Electron., **66**, 1 (2019). DOI: 10.1016/j.pquantelec.2019.05.002

[2] M. Kawabe, T. Ueda, Jpn. J. Appl. Phys., **26** (6A), L944 (1987). DOI: 010.1143/JJAP.26.L944

[3] A.Y. Liu, J. Peters, X. Huang, D. Jung, J. Norman, M.L. Lee, A.C. Gossard, J.E. Bowers, Opt. Lett., **42** (2), 338 (2017). DOI: 10.1364/OL.42.000338

[4] A. Sakanas, E. Semenova, L. Ottaviano, J. Mørk, K. Yvind, Microelectron. Eng., **214**, 93 (2019). DOI: 10.1016/j.mee.2019.05.001

[5] A. Osada, Y. Ota, R. Katsumi, M. Kakuda, S. Iwamoto, Y. Arakawa, Phys. Rev. Appl., **11** (2), 024071 (2019). DOI: 10.1103/PhysRevApplied.11.024071

[6] M. Borg, H. Schmid, K.E. Moselund, G. Signorello, L. Gignac, J. Bruley, C. Breslin, P. Das Kanungo, P. Werner, H. Riel, Nano Lett., **14** (4), 1914 (2014). DOI: 10.1021/nl404743j.

[7] J. Vukajlovic-Plestina, W. Kim, L. Ghisalberti, G. Varnavides, G. Tütüncuoglu, H. Potts, M. Friedl, L. Güniat, W.C. Carter, V.G. Dubrovskii, A. Fontcuberta i Morral, Nat. Commun., **10** (1), 869 (2019). DOI: 10.1038/s41467-019-08807-9

[8] D.V. Viazmitinov, Y. Berdnikov, S. Kadkhodazadeh, A. Dragunova, N. Sibirev, N. Kryzhanovskaya, I. Radko, A. Huck, K. Yvind, E. Semenova, Nanoscale, **12** (46), 23780 (2020). DOI: 10.1039/D0NR05779G

[9] I. Melnichenko, E. Moiseev, N. Kryzhanovskaya, I. Makhov, A. Nadtochiy, N. Kalyuznyy, V. Kondratev, A. Zhukov, Nanomaterials, **12** (23), 4213 (2022). DOI: 10.3390/nano12234213

[10] S. Tiwari, *Compound semiconductor device physics* (Academic Press, N.Y., 1992).

[11] H.P. Lei, H.Z. Wu, Y.F. Lao, M. Qi, A.Z. Li, W.Z. Shen, J. Cryst. Growth, **256** (1-2), 96 (2003). DOI: 10.1016/S0022-0248(03)01345-9

[12] I. Vurgaftman, J.R. Meyer, L.R. Ram-Mohan, J. Appl. Phys., **89** (11), 5815 (2001). DOI: 10.1063/1.1368156

Translated by D.Safin